Chemical Science

ROYAL SOCIETY OF CHEMISTRY

EDGE ARTICLE

View Article Online
View Journal | View Issue

Cite this: *Chem. Sci.*, 2020, **11**, 3680

All publication charges for this article have been paid for by the Royal Society of Chemistry

Site-specific growth of MOF-on-MOF heterostructures with controllable nano-architectures: beyond the combination of MOF analogues†

Chao Liu,[a] Lina Lin,[b] Qiang Sun,[c] Jing Wang,[a] Rong Huang,[b] Wenyi Chen,[a] Shumin Li,[a] Jingjing Wan,*[a] Jin Zou *[cd] and Chengzhong Yu *[ae]

The integration of different metal–organic frameworks (MOFs) into one system has led to the recent combinatorial innovation of various MOF-on-MOF hybrids; however control over their site-specific growth beyond MOF analogues remains challenging. In this work, a site-specific epitaxial-growth strategy is developed to synthesize MOF-on-MOF heterostructures comprised of two MOFs with totally different compositions. A guest MOF (ZIF-8) is epitaxially grown on the specific {110} facets of a host MOF (MIL-125). Moreover, the position of ZIF-8 growth on MIL-125 is also selectable by using MIL-125 hosts with {110} facets exposed on either the corner or side surface. Consequently, two MIL-125@ZIF-8 heterostructures with elaborately designed different architectures are synthesized. Benefiting from the high adsorption capacity of ZIF-8 and the photocatalytic activity of MIL-125, the MIL-125@ZIF-8 heterostructures demonstrate synergistically enhanced photocatalytic performance compared to single MOF subunits. Moreover, the corner growth leads to higher activity than the side growth of the MIL-125@ZIF-8 heterostructures. Our contribution paves the way for the rational design of composite MOFs with tunable compositions and nanostructures using the crystal engineering approach.

Received 22nd January 2020
Accepted 4th March 2020

DOI: 10.1039/d0sc00417k

rsc.li/chemical-science

Introduction

Growth of a guest structure on a specific site of a host is a powerful approach for constructing nanomaterials with complex compositions and architectures, from which distinctive nanomaterials with a variety of compositional and/or structural combinations have been developed.[1–4] For example, Jia *et al.*[5] demonstrated a wet-chemistry route for the selective growth of crystalline ceria at the tip of gold nanorods due to the reduced surfactant density at the tip side compared to the body side. Wu and co-workers[6] synthesized colloidal SiO_2 rings by selective growth of silica on the side surface of polymer discs with the top and bottom surfaces covered by insoluble polymers. Huang *et al.*[7] also achieved the site-specific growth of Au–Pd alloy horns at the ends of Au nanorods *via* the epitaxial growth. The nanocomposites produced by the site-specific growth approach have shown superior performance in the fields of energy storage/conversion, separation, heterogeneous catalysis and biomedicine compared to single building blocks.[8–10]

Metal–organic frameworks (MOFs), an appealing class of porous crystalline materials, have been widely investigated due to their excellent physicochemical features.[11–15] Introducing other functional species such as nanoparticles,[16–18] enzymes,[19–21] DNA[22] and polymers[23,24] has endowed MOFs with additional properties. In these hybrid MOFs, guest objects are generally encapsulated in the MOFs' framework without site selectivity. The growth of MOFs on various substrates, *e.g.*, $Cu(OH)_2$ foil, Ni foam and carbon fiber cloth, was also reported usually with random orientation.[25–27] Recently, an intriguing integration, named MOF-on-MOF, was developed by growing guest MOFs on pre-formed host MOFs.[28–39] This strategy creates enormous opportunities for the construction of novel MOF hybrids with unprecedented structural diversities and improved properties. To date, epitaxial growth has been the most efficient way to achieve the site-specific growth of MOF-on-MOF. For example, anisotropic hybridization of single-crystalline MOFs *via* face-selective epitaxial growth was reported for asymmetric MOF-on-MOF heterostructures.[40–42] Recently, Oh's group reported

[a]School of Chemistry and Molecular Engineering, East China Normal University, Shanghai 200241, P. R. China. E-mail: jjwan@chem.ecnu.edu.cn; czyu@chem.ecnu.edu.cn

[b]Key Laboratory of Polar Materials and Devices (MOE), Department of Electronics, East China Normal University, Shanghai 200241, P. R. China

[c]Materials Engineering, University of Queensland, Brisbane, Queensland 4072, Australia. E-mail: j.zou@uq.edu.au

[d]Centre for Microscopy and Microanalysis, University of Queensland, Brisbane, Queensland 4072, Australia

[e]Australian Institute for Bioengineering and Nanotechnology, The University of Queensland, Brisbane, Queensland 4072, Australia. E-mail: c.yu@uq.edu.au

† Electronic supplementary information (ESI) available. See DOI: 10.1039/d0sc00417k

isotropic and anisotropic growth of secondary MOFs on a pre-synthesized MOF template to form MOF-on-MOF with controllable nanostructures.[32] However, in these reports, guest MOFs have been grown on their analogues as the host with either the same metal ions or ligands *via* epitaxial growth, limiting the structural and compositional diversity of MOF-on-MOF hybrids. Another method is using surfactants to enhance the interaction between the guest and host MOFs, through which MOFs with totally different compositions can be integrated. Unfortunately guest MOFs were randomly adhered on host MOFs without site selectivity.[37,38] Therefore, controllable growth of guest MOFs on the specific site of host MOFs with totally different components for the synthesis of MOF-on-MOF heterostructures is rarely reported.

Herein, a site-specific epitaxial-growth strategy is used to synthesize elaborately designed MOF-on-MOF heterostructures. Two tetragonal structured Ti-based MOFs (MIL-125, space group of $I4/mmm$ with the lattice parameters of $a = 18.65$ Å and $c = 18.14$ Å)[43] with cake-like and box-like morphologies (named $_c$MIL-125 and $_b$MIL-125) are chosen as the hosts. Their {110} facets are respectively exposed on the corner and side surfaces, as illustrated in Scheme 1A and B. Then, a cubic structured Zn-based MOF (ZIF-8) (space group of $I\bar{4}3m$ with a lattice parameter of $a = 16.99$ Å)[44] is selected as the guest to epitaxially grow on the {110} surfaces of MIL-125 due to their small lattice mismatches on the specific interfaces. Scheme 1C illustrates theoretical lattice mismatches in the $\{110\}_{\text{MIL-125}}/\{001\}_{\text{ZIF-8}}$ interface, in which the lattice mismatch between $d_{(002)\text{MIL-125}}$ and $d_{(200)\text{ZIF-8}}$ is ~6.3% and that between $2d_{(110)\text{MIL-125}}$ and $3d_{(020)\text{ZIF-8}}$ is only ~2.6%, far below the lattice mismatch allowed for epitaxial growth (<15%).[45] The possible molecular structure at the overlaid interface is proposed in Scheme S1.† Notably, the epitaxial relationship between ZIF-8 and MIL-125 is established for the first time, which is never observed before. Ultimately, two well-designed MIL-125@ZIF-8 heterostructures, as illustrated in Scheme 1A and B, were generated, the morphologies and compositions of which are different from all reported MOF-on-MOF hybrids. To the best of our knowledge, site-specific growth of MOF-on-MOF heterostructures with controllable nano-architectures without using the combination of MOF analogues is demonstrated for the first time.

Results and discussion

As a representative demonstration, the structure of the $_c$MIL-125@ZIF-8 heterostructure with ZIF-8 grown on the corner of $_c$MIL-125 was first investigated. $_c$MIL-125 particles synthesized *via* a solvothermal method[43] (see the Experimental section) were used as the host. As shown in the field-emission scanning electron microscopy (SEM) images (Fig. S1a and b†), the $_c$MIL-125 particles are highly dispersed with an average length of ~650 nm and thickness of ~175 nm. Transmission electron microscopy (TEM) images (Fig. S1c†) show the solid nature of these cake-like particles. The X-ray diffraction (XRD) pattern confirms the high crystallinity of $_c$MIL-125 (Fig. S2†), in agreement with the structure reported in the literature.[43]

Subsequently, ZIF-8 nanocrystals were directly grown onto $_c$MIL-125 without using surfactants, forming MOF-on-MOF heterostructures. Fig. 1a shows a typical SEM image of the resultant $_c$MIL-125@ZIF-8, demonstrating a unique and uniform morphology. Fig. 1b shows a magnified SEM image showing that cubic structured ZIF-8 nanoparticles (diameters of ~200 nm) are selectively adhered on the four corners of $_c$MIL-125 with good mechanical robustness, which is evidenced by the well-maintained structure after sonication (Fig. S3†). As can be seen, the grown ZIF-8 nanoparticles have particular facets oriented to the host $_c$MIL-125, as marked by red dashed lines. Fig. 1c and S4† show TEM images and show the projection of

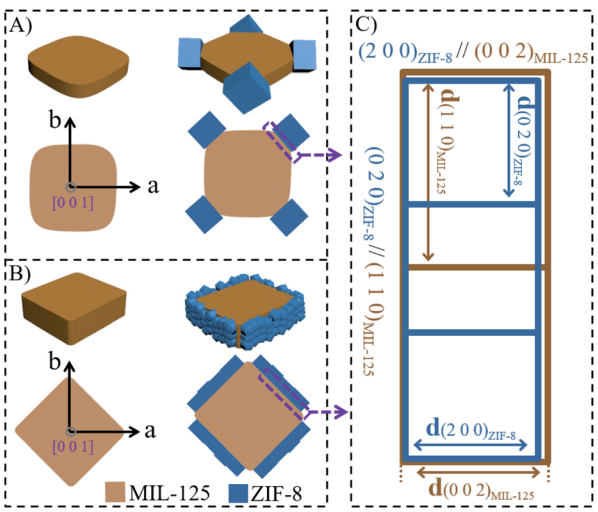

Scheme 1 Schematic illustration of site-selective epitaxial-growth of ZIF-8 on MIL-125. Selective growth of ZIF-8 (A) on the corner {110} facets of $_c$MIL-125 and (B) on the side {110} facets of $_b$MIL-125. (C) Schematic diagram showing near coherence of the planes at the MIL-125/ZIF-8 interface.

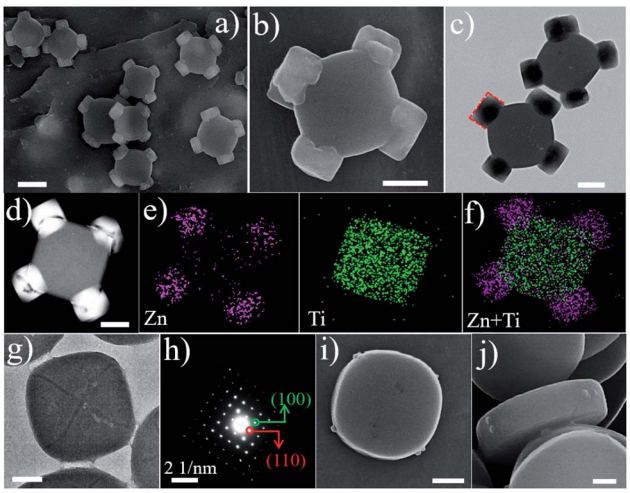

Fig. 1 (a and b) SEM images, (c) TEM image, (d) STEM image, and (e and f) elemental mapping images of $_c$MIL-125@ZIF-8; (g) TEM image and (h) SAED patterns of $_c$MIL-125. (i and j) SEM images of the sample after growth of ZIF-8 on $_c$MIL-125 for 2 min. The scale bars are 500 nm (a), 200 nm (b, c, d, and i) and 100 nm (g and j).

ZIF-8 nanoparticles with the host $_c$MIL-125, in which the ZIF-8 projections are well faceted with the host. Fig. 1d shows a high-angle annular dark-field image taken in the scanning transmission electron microscopy mode (HAADF-STEM) and shows a much brighter contrast of ZIF-8 nanoparticles. This indicates that the ZIF-8 nanoparticles grown on the corners contain relatively heavier elements than the host. Fig. 1e show elemental maps of Zn and Ti, from which ZIF-8 containing Zn on four corners and the host $_c$MIL-125 containing Ti can be seen. Fig. 1f shows a superimposed elemental map showing the composition distribution. In the $_c$MIL-125@ZIF-8 heterostructure, four Zn-enriched faceted nanoparticles are preferentially formed on the corners of the Ti-enriched $_c$MIL-125 host.

Inductively coupled plasma optical emission spectrometry (ICP-OES) was employed to determine the contents of ZIF-8 and $_c$MIL-125 in $_c$MIL-125@ZIF-8, which are calculated to be ~30.6% and 69.4% based on the Ti/Zn mass ratio (~1.83/1). Fig. S5† shows Fourier transform infrared (FTIR) spectra of $_c$MIL-125@ZIF-8, in which the bands at 2929 cm^{-1}, 1379 cm^{-1} and 1572 cm^{-1} are assigned to the CH_3^- group of 2-MeIM in ZIF-8 and the carboxyl group of ATA in $_c$MIL-125, respectively. Fig. 2a shows the XRD pattern of $_c$MIL-125@ZIF-8 and shows both $_c$MIL-125 and ZIF-8 diffraction peaks. The N_2 adsorption–desorption isotherms (Fig. S6†) of ZIF-8, $_c$MIL-125 and $_c$MIL-125@ZIF-8 demonstrate their microporous structures. The BET surface areas and pore volumes are illustrated in Table S1.†

To understand the formation mechanism of $_c$MIL-125@ZIF-8 heterostructures, we investigated intermediate steps during the formation of $_c$MIL-125@ZIF-8 heterostructures. Fig. 1g shows a typical TEM image of a host $_c$MIL-125 nanoparticle, and Fig. 1h shows the corresponding selected area electron diffraction (SAED) pattern. By correlating Fig. 1g and h, the side facets of the $_c$MIL-125 can be assigned as the {100} planes, and the corner sides as the {110} planes. The SAED pattern (Fig. S7†) of $_c$MIL-125@ZIF-8 shows only the diffraction spots corresponding to MIL-125. The absence of diffraction spots of ZIF-8 may be because the crystalline structure of ZIF materials was easily damaged and converted into an amorphous structure under electron beam irradiation.[46,47] Fig. 1i and j show SEM images of the initial growth of ZIF-8 on the cake-like $_c$MIL-125 host (products collected after 2 min of ZIF-8 growth). Some nucleates are clearly seen only at the corner of the host $_c$MIL-125, rather than on the side or top surface, indicating that only {110} surfaces of MIL-125 are the nucleation sites for growing ZIF-8.

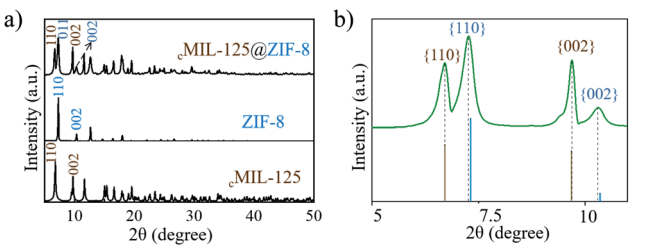

Fig. 2 (a and b) XRD patterns of $_c$MIL-125@ZIF-8. (b) The enlarged pattern of (a) in the range of 2θ from 5–12°.

To further study the formation of ZIF-8 on $_c$MIL-125, the samples after 2 min of ZIF-8 growth in the presence of $_c$MIL-125 as the substrate were directly observed by SEM without centrifugation and methanol washing treatment, showing nucleation of ZIF-8 on the corner of $_c$MIL-125, while ZIF-8 nanocrystals not connected to $_c$MIL-125 formed through homogeneous nucleation were not observed (Fig. S8†). Then, $_c$MIL-125 particles were added after homogeneous nucleation and growth of ZIF-8 for 2 and 5 min. The collected sample at 2 min showed the coexistence of dodecahedral ZIF-8 particles with an average diameter of ~820 nm, presumably generated by homogeneous nucleation and growth of ZIF-8 itself, and small ZIF-8 nanocrystals with open holes, possibly through heterogeneous nucleation on the corners of $_c$MIL-125 and then detachment (Fig. S9†). When the pre-nucleation time of ZIF-8 prolonged to 5 min, only a mixture of dodecahedral ZIF-8 particles and $_c$MIL-125 was observed (Fig. S10†). These results indicate that the growth of $_c$MIL-125@ZIF-8 is through heterogeneous nucleation of ZIF-8 clusters on the {110} facets of MIL-125. However, if $_c$MIL-125 templates were added after the homogeneous nucleation of ZIF-8, the probability of homogeneous nucleation and growth of ZIF-8 is increased, leading to a mixture of products.

Without the assistance of surfactants, it has been reported that the crystal growth of ZIF-8 starts with formation of cubes exposing six {001} facets,[48,49] from which thermodynamically more stable rhombic dodecahedra with twelve {110} facets are finally obtained. Consistent with the literature, in our experiments the direct growth of ZIF-8 in methanol without the $_c$MIL-125 host resulted in the formation of ZIF-8 nanoparticles with a dodecahedral morphology, as shown in Fig. S11 and S12.† In contrast, with $_c$MIL-125 as the host and its exposed {110} surfaces, cubic structured ZIF-8 may be epitaxially grown on the {110} surfaces of $_c$MIL-125 due to their small lattice mismatch at the $\{001\}_{ZIF\text{-}8}/\{110\}_{cMIL\text{-}125}$ interface. The epitaxial relationship of $\{100\}_{ZIF\text{-}8}//\{001\}_{cMIL\text{-}125}$ and $\{010\}_{ZIF\text{-}8}//\{110\}_{cMIL\text{-}125}$ (proposed in Scheme 1C) can be evidenced by SEM and TEM (Fig. 1b and c), indicating that the growth behavior of ZIF-8 crystals is manipulated due to the existence of the {110} surfaces of $_c$MIL-125.

To further clarify the epitaxial relationship, we carefully investigated the XRD patterns of $_c$MIL-125@ZIF-8 heterostructures. Fig. 2b shows an enlarged XRD pattern, in which the positions of diffraction peaks are compared with the positions of standard diffraction peaks. The diffraction peaks corresponding to the $_c$MIL-125 host fit well with standard diffraction peaks, suggesting that the lattice parameters of the $_c$MIL-125 host are retained after the growth of ZIF-8. In contrast, the diffraction peaks corresponding to the ZIF-8's {110} and {002} planes have slightly shifted to a smaller angle when compared with their standard peaks, indicating the lattice expansion of ZIF-8 when they are grown on $_c$MIL-125. From these results, the calculated residual lattice mismatches between $d_{(200)ZIF\text{-}8}$ and $d_{(002)MIL\text{-}125}$ and between $3d_{(020)ZIF\text{-}8}$ and $2d_{(110)MIL\text{-}125}$ decreased (4.8% and 2.1%) almost proportionally compared to the theoretical values (6.3% and 2.6%), implying that the structural deformation occurred during the epitaxial growth of ZIF-8 on $_c$MIL-125. Similar observations were reported in other hetero-

epitaxially grown crystals.[25,50] By growth of ZIF-8 with a larger diameter of ~500 nm (Fig. S13†), the lattice expansion decreased from 0.50% to 0.27%, indicating that the lattice parameters are more reminiscent of the pure ZIF-8 (Fig. S14†).

To further support the epitaxial growth of ZIF-8 on the {110} surfaces of MIL-125, box-like $_b$MIL-125 particles were also synthesized as the host, in which the side facets are {110} planes; thus the ZIF-8 nanoparticles are expected to grow on the side surfaces of the $_b$MIL-125 hosts. The SEM and TEM images (Fig. S15†) of $_b$MIL-125 confirmed the box-like morphology with an average edge length of ~350 nm and thickness of ~250 nm. Fig. S16† shows the XRD pattern of $_b$MIL-125 showing good crystallinity. Fig. 3a and S17† show SEM images and show that ZIF-8 nanocrystals are indeed selectively grown on the side surface of $_b$MIL-125 as expected. Fig. 3b and 2c show SEM and TEM images of typical $_b$MIL-125@ZIF-8 heterostructures, showing ZIF-8 nanoparticles covered on the side surfaces of $_b$MIL-125 with a thickness of ~100 nm. Fig. 3d–f show the HAADF-STEM image, elemental maps and superimposed map of a typical $_b$MIL-125@ZIF-8 heterostructure, from which the element distribution of Zn and Ti in ZIF-8 and MIL-125 can be clearly distinguished. The contents of ZIF-8 and $_b$MIL-125 in $_b$MIL-125@ZIF-8 were calculated to be ~33.5% and 66.5% based on ICP measurements, respectively. The N_2 sorption isotherms of $_b$MIL-125 and $_b$MIL-125@ZIF-8 are shown in Fig. S6† with specific surface areas and pore volumes listed in Table S1.†

Fig. S18 and S19† show the XRD pattern and FT-IR spectra, confirming the co-existence of crystalline ZIF-8 and MIL-125 in $_b$MIL-125@ZIF-8 heterostructures. By comparing the positions of diffraction peaks of $_b$MIL-125@ZIF-8 with standard ones in the enlarged XRD patterns (Fig. S20†), the lattice expansion of ZIF-8 and decreased lattice mismatches between ZIF-8 and $_b$MIL-125 are also observed, consistent with those observed in the $_c$MIL-125@ZIF-8 heterostructure. Similar to the investigation on $_c$MIL-125@ZIF-8, the intermediate step of the ZIF-8 growth was investigated. Fig. 3g and h show the TEM image and corresponding SAED pattern of a pure $_b$MIL-125 host, and their correlation confirms that the side facets of $_b$MIL-125 are indeed {110} planes. Fig. 3i and j show SEM images of products after 2 min of growing ZIF-8 and show that ZIF-8 nucleates are formed only on the side surfaces of $_b$MIL-125. These observations further verify the unique epitaxial growth of ZIF-8 on MIL-125 with the defined orientation, and the position of ZIF-8 growth can be controlled in the resultant MOF-on-MOF heterostructures.

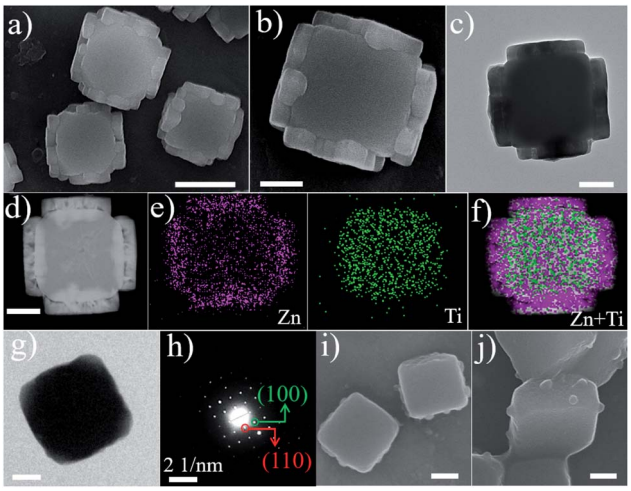

Fig. 3 (a and b) SEM images, (c) TEM image, (d) STEM image, and (e and f) elemental mapping images of $_b$MIL-125@ZIF-8; (g) TEM image and (h) SAED patterns of $_b$MIL-125. (i and j) SEM images of the sample after growth of ZIF-8 on $_b$MIL-125 for 2 min. The scale bars are 500 nm (a), 200 nm (b, c, d, i, and j) and 100 nm (g).

To demonstrate the importance of selection of host and guest MOFs for epitaxial growth, MIL-125 or ZIF-8 was selectively replaced by other two typical MOFs {MIL-88B (space group of $P6_3/mmc$ with lattice parameters of $a = b = 11.1075$ Å and $c = 19.0925$ Å) and HKUST-1 ($Fm\bar{3}m$ with lattice parameters of $a = b = c = 26.343$ Å)}. The largest lattice mismatch of MIL-88B (host)/ZIF-8 (guest) and MIL-125 (host)/HKUST-1 (guest) was calculated to be 34.6% and 31.1%, respectively. The results (Fig. S21–S24†) showed that ZIF-8 and HKUST-1 were grown by themselves with the existence of MIL-88B and MIL-125, respectively, resulting in the mixture of host and guest MOFs. It is reported that the lattice mismatch between two crystals should be less than 15% for epitaxial growth.[44] Our observations are consistent with literature reports, indicating that the selection of host–guest MOFs with small lattice mismatch is extremely important for epitaxial growth of MOF-on-MOF hybrids.

When using an octahedral MIL-125 (denoted as $_o$MIL-125) with eight exposed {111} facets, the individual growth of ZIF-8 was observed without the MOF-on-MOF heterostructure formed (Fig. S25 and S26†), indicating the necessity of the {110} facets in MIL-125 to allow the epitaxial growth of ZIF-8. Another synthesis similar to that of $_c$MIL-125@ZIF-8 was also conducted, except for adding Zn^{2+} first and then 2-MeIM. The obtained sample showed an inhomogeneous structure with partial MIL-125 anchored by ZIF-8 (Fig. S27†), different from $_c$MIL-125@ZIF-8. It is reported that the {110} facets of MIL-125 have a high content of exposed Ti–O clusters.[51] Our result suggests that the interaction between 2-MeIM and Ti–O clusters exposed on {110} facets of MIL-125 is also associated with the site-selective growth of $_c$MIL-125@ZIF-8. A possible molecular structure at the overlaid interface of $\{110\}_{MIL\text{-}125}/\{001\}_{ZIF\text{-}8}$ is proposed in Scheme S1† on the basis of our experimental observations and literature reports.[51,52] The exposed Ti–O nodes could be fully utilized with one Ti–O cluster connected with 2-MeIM to induce the growth of ZIF-8, leaving one Zn^{2+} cluster not connected to the Ti–O node at the interface. Nevertheless, the actual interfacial structure of $\{110\}_{MIL\text{-}125}/\{001\}_{ZIF\text{-}8}$ could be different from that reported based on a single structure, which is worth investigating in future studies.

In general, heterostructures with complementary properties often enhance their performance in applications. It has been reported that ZIF-8 is an adsorbent,[15] while MIL-125 is a promising photocatalyst.[40,53] Hypothetically, the MIL-125@ZIF-8 hetero-structures may enrich molecules such as pollutants in solution through ZIF-8 and then degrade the enriched molecules through MIL-125 by photocatalysis within one particle. For this reason, we investigated the performance of MIL-

125@ZIF-8 heterostructures by using photocatalytic degradation of orange II (a dye pollutant) as a model reaction, using ZIF-8, $_c$MIL-125 and $_b$MIL-125 as the control (Fig. 4a, S28†). The catalysts/orange II suspension was stirred in the dark for 60 min to establish the adsorption equilibrium, after which photocatalysis reaction was initiated by visible light irradiation. As shown in Fig. 4b, ZIF-8 showed an obviously higher adsorption ratio of 51.8% than $_c$MIL-125 (6.9%) and $_b$MIL-125 (6.0%) after 60 min adsorption in the dark. This difference is attributed to the electrostatic attraction between positively charged ZIF-8 (Fig. S29†) and negatively charged dye molecules, while MIL-125 has a negatively charged surface (Fig. S30 and S31†) which causes electrostatic repulsion of orange II. Considering the limited pore window (0.34 nm) of ZIF-8,[54] the adsorption of the dye by ZIF-8 is presumably by surface electrostatic interaction. Notably, $_c$MIL-125@ZIF-8 and $_b$MIL-125@ZIF-8 possessed enhanced adsorption of orange II (21.4% and 22.9%, respectively) compared to pure MIL-125, which can be attributed to the presence of ZIF-8 in the heterostructures.

When the photocatalytic reaction was switched on, almost no orange II was removed in the absence of any materials during the whole process. $_c$MIL-125@ZIF-8 exhibited fast degradation of orange II with a removal rate of ~97.3% in 120 min under visible light irradiation, higher than that of $_c$MIL-125 (54.6%). Similarly, improved dye degradation efficiency was also observed in $_b$MIL-125@ZIF-8 (86.0%) compared to that in $_b$MIL-125 (57.3%). The slightly higher removal efficiency of $_b$MIL-125 than $_c$MIL-125 may be ascribed to the more exposed metal clusters offered by the {110} facets and more surface energy with higher activity, consistent with the reported work.[51] ZIF-8 showed a poor photocatalytic activity with only 8.4% of orange II removed during the photocatalytic stage, which may be ascribed to the weak absorbance of visible light (Fig. S32†). In addition, the degradation efficiency of the ZIF-8/MIL-125 mixture by directly mixing ZIF-8 and MIL-125 with the same ratio was obviously lower than that of the MIL-125@ZIF-8 heterostructures, indicating that the contact between MIL-125 and ZIF-8 is important for improving the degradation performance. The higher total organic carbon (TOC) removal rate of the MIL-125@ZIF-8 heterostructures than other samples (Fig. S33†) further indicates their enhanced performance. The active species in the MIL-125@ZIF-8 catalytic system was proved to be superoxide radicals by electron paramagnetic resonance (EPR) measurements (Fig. S34 and S35†) without hydroxyl radicals being detected. The result is in accordance with a previous report that superoxide radicals are the dominant species generated by MIL-125 under visible light irradiation.[43] The superoxide radical levels were similar in MIL-125@ZIF-8 and MIL-125/ZIF-8 mixtures, indicating that the dye adsorption difference is responsible for the dye degradation behaviour observed in different groups (Fig. 4a).

Collectively, MIL-125@ZIF-8 heterostructures show synergistically enhanced photocatalytic degradation of orange II, significantly higher than the sum of MIL-125 and ZIF-8 contribution individually and the mixture of ZIF-8/MIL-125. It is suggested that the photocatalytic activity of pure MIL-125 is hindered for molecules such as orange II with poor adsorption efficiency. For MIL-125@ZIF-8 heterostructures, the photocatalytic MIL-125 moiety generates superoxide radicals under light irradiation, while the positively charged ZIF-8 moiety reduces the negative surface potential of MIL-125 which facilitates the adsorption of negatively charged orange II. Consequently, the local concentration of orange II is increased and the kinetics of the catalytic reaction are accelerated. It can also increase the contact rate between the dye and active species, thus promoting the dye degradation.[18,38,55–57] The relatively higher performance of $_c$MIL-125@ZIF-8 than $_b$MIL-125@ZIF-8 is possibly attributed to its higher portion of the non-enclosed structure, suggesting that control over the site of ZIF-8 growth is also important to finely tune the performance of MOF-on-MOF heterostructures.

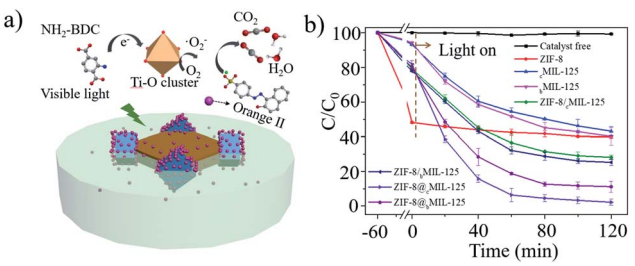

Fig. 4 (a) Illustration of the enhanced photocatalytic degradation process towards orange II using ZIF-8@MIL-125. (b) Degradation efficiency of ZIF-8, $_c$MIL-125, $_b$MIL-125, $_c$MIL-125/ZIF-8, $_b$MIL-125/ZIF-8, $_b$MIL-125, $_c$MIL-125@ZIF-8 and $_b$MIL-125@ZIF-8.

Conclusions

In summary, controllable synthesis of MOF-on-MOF heterostructures with well-designed architectures is demonstrated *via* an orientation-specific and position-selectable epitaxial-growth strategy. The guest ZIF-8 is epitaxially grown on the {110} facets of the host MIL-125. Meanwhile, the position of ZIF-8 growth on MIL-125 can be controlled on either the corner or side surface, generating two MIL-125@ZIF-8 heterostructures. Benefiting from the synergistic effect between the enrichment contribution of ZIF-8 and photocatalytic activity of MIL-125, the synthesized MIL-125@ZIF-8 heterostructures demonstrate superior performance in photocatalysis compared to single MOFs. The findings may pave the way for the construction of distinctive MOF hybrids for various applications.

Conflicts of interest

There are no conflicts to declare.

Acknowledgements

The authors acknowledge support from the Australian Research Council, the Australian National Fabrication Facility-Queensland Node (ANFFQ), Microscopy Australia, the National Natural Science Foundation of China (NSFC 21905092, 51908218, and 21705107), Shanghai Science and Technology Foundation (Grant No. 19JC1412100) and a project funded by the China Postdoctoral Science Foundation.

Notes and references

1 W. Andreas and H. E. M. Axel, Janus Particles: Synthesis, Self-Assembly, Physical Properties, and Applications, *Chem. Rev.*, 2013, **7**, 5194.

2 J. Hu, S. X. Zhou, Y. Y. Sun, X. S. Fang and L. M. Wu, Fabrication, properties and applications of Janus particles, *Chem. Soc. Rev.*, 2012, **41**, 4356.

3 S. Jiang, Q. Chen, M. Tripathy, E. Luijten, K. S. Schweizer and S. Granick, Janus particle synthesis and assembly, *Adv. Mater.*, 2010, **22**, 1060.

4 S. E. Habas, P. D. Yang and T. Mokari, Selective Growth of Metal and Binary Metal Tips on CdS Nanorods, *J. Am. Chem. Soc.*, 2008, **130**, 3294.

5 H. L. Jia, A. X. Du, H. Zhang, J. H. Yang, R. B. Jiang, J. F. Wang and C. Y. Zhang, Site-Selective Growth of Crystalline Ceria with Oxygen Vacancies on Gold Nanocrystals for Near-Infrared Nitrogen Photofixation, *J. Am. Chem. Soc.*, 2019, **141**, 5083.

6 Y. Y. Wu, Z. Luo, B. Liu and Z. Z. Yang, Colloidal Rings by Site-Selective Growth on Patchy Colloidal Disc Templates, *Angew. Chem., Int. Ed.*, 2017, **56**, 9807.

7 J. F. Huang, Y. H. Zhu, M. Lin, Q. X. Wang, L. Zhao, Y. Yang, K. X. Yao and Y. Han, Site-Specific Growth of Au-Pd Alloy Horns on Au Nanorods: A Platform for Highly Sensitive Monitoring of Catalytic Reactions by Surface Enhancement Raman Spectroscopy, *J. Am. Chem. Soc.*, 2013, **135**, 8552.

8 P. Zhang, L. Yu and X. W. Lou, Construction of Heterostructured Fe_2O_3-TiO_2 Microdumbbells for Photoelectrochemical Water Oxidation, *Angew. Chem., Int. Ed.*, 2018, **57**, 15076.

9 X. L. Pan, Z. L. Fan, W. Chen, Y. J. Ding, H. Y. Luo and X. H. Bao, Enhanced ethanol production inside carbon-nanotube reactors containing catalytic particles, *Nat. Mater.*, 2007, **6**, 507.

10 P. L. Abbaraju, A. K. Meka, H. Song, Y. N. Yang, M. Jambhrunkar, J. Zhang, C. Xu, M. H. Yu and C. Z. Yu, Asymmetric silica nanoparticles with tunable head-tail structures enhance hemocompatibility and maturation of immune cells, *J. Am. Chem. Soc.*, 2017, **139**, 6321.

11 H. Furukawa, K. E. Cordova, M. O'Keeffe and O. M. Yaghi, The Chemistry and Applications of Metal-Organic Frameworks, *Science*, 2013, **341**, 974.

12 O. M. Yaghi, M. O'Keeffe, N. W. Ockwig, H. K. Chae, M. Eddaoudi and J. Kim, Reticular Synthesis and The Design of New Materials, *Nature*, 2003, **423**, 705.

13 J. Y. Lee, O. K. Farha, J. Roberts, K. A. Scheidt, S. T. Nguyen and J. T. Hupp, Metal-Organic Framework Materials as Catalysts, *Chem. Soc. Rev.*, 2009, **38**, 1450.

14 J. D. Xiao and H. L. Jiang, Metal-Organic Frameworks for Photocatalysis and Photothermal Catalysis, *Acc. Chem. Res.*, 2019, **52**, 356.

15 J. R. Li, J. Sculley and H. C. Zhou, Metal-Organic Frameworks for Separations, *Chem. Rev.*, 2012, **112**, 869.

16 G. Lu, S. Z. Li, Z. Guo, O. K. Farha, B. G. Hauser, X. Y. Qi, Y. Wang, X. Wang, S. Y. Han, X. G. Liu, J. S. DuChene, H. Zhang, Q. C. Zhang, X. D. Chen, J. Ma, S. C. J. Loo, W. Wei, Y. H. Yang, J. T. Hupp and F. W. Huo, Imparting Functionality to A Metal-Organic Framework Material by Controlled Nanoparticle Encapsulation, *Nat. Chem.*, 2012, **4**, 310.

17 M. T. Zhao, K. Yuan, Y. Wang, G. D. Li, J. Guo, L. Gu, W. P. Hu, H. J. Zhao and Z. Y. Tang, Metal-Organic Frameworks as Selectivity Regulators for Hydrogenation Reactions, *Nature*, 2016, **539**, 76.

18 Q. H. Yang, Q. Xu and H. L. Jiang, Metal-Organic Frameworks Meet Metal Nanoparticles: Synergistic Effect for Enhanced Catalysis, *Chem. Soc. Rev.*, 2017, **46**, 4774.

19 X. Z. Lian, E. Joseph, Q. Wang, J. L. Li, S. Banerjee, C. Lollar, X. Wang and H. C. Zhou, Enzyme-MOF (Metal-Organic Framework) Composites, *Chem. Soc. Rev.*, 2017, **46**, 3386.

20 F. S. Liao, W. S. Lo, Y. S. Hsu, C. C. Wu, S. C. Wang, F. K. Shieh, J. V. Morabito, L. Y. Chou, K. C. W. Wu and C. K. Tsung, Shielding against Unfolding by Embedding Enzymes in Metal-Organic Frameworks via a de Novo Approach, *J. Am. Chem. Soc.*, 2017, **139**, 6530.

21 W. H. Chen, M. Vázquez-González, A. Zoabi, R. A. Rezip and I. Willner, Biocatalytic Cascades Driven by Enzymes Encapsulated in Metal-Organic Framework Nanoparticles, *Nat. Catal.*, 2018, **1**, 689.

22 J. S. Kahn, L. Freage, N. Enkin, M. A. A. Garcia and I. Willner, Stimuli-Responsive DNA-Functionalized Metal-Organic Frame-works (MOFs), *Adv. Mater.*, 2016, **29**, 1602782.

23 Y. W. Peng, M. T. Zhao, B. Chen, Z. C. Zhang, Y. Huang, F. N. Dai, Z. C. Lai, X. Y. Cui, C. L. Tan and H. Zhang, Hybridization of MOFs and COFs: A New Strategy for Construction of MOF@COF Core-Shell Hybrid Materials, *Adv. Mater.*, 2018, **30**, 1705454.

24 F. M. Zhang, J. L. Sheng, Z. D. Yang, X. J. Sun, H. L. Tang, L. Meng, H. Dong, F. C. Shen, J. Liu and Y. Q. Lan, Rational Design of MOF/COF Hybrid Materials for Photocatalytic H_2 Evolution in the Presence of Sacrificial Electron Donors, *Angew. Chem., Int. Ed.*, 2018, **57**, 12106.

25 P. Falcaro, K. Okada, T. Hara, K. Ikigaki, Y. Tokudome, A. W. Thornton, A. J. Hill, T. Williams, C. Doonan and M. Takahashi, Centimetre-Scale Micropore Alignment in Oriented Polycrystal-line Metal-Organic Framework Films via Heteroepitaxial Growth, *Nat. Mater.*, 2017, **16**, 342.

26 K. Jayaramulu, K. K. R. Datta, C. Rösler, M. Petr, M. Otyepka, R. Zboril and R. A. Fischer, Biomimetic Superhydrophobic/Superoleophilic Highly Fluorinated Graphene Oxide and ZIF-8 Composites for Oil-Water Separation, *Angew. Chem., Int. Ed.*, 2016, **55**, 1178.

27 J. J. Duan, S. Chen and C. Zhao, Ultrathin Metal-Organic Framework Array for Efficient Electrocatalytic Water Splitting, *Nat. Commun.*, 2017, **8**, 15341.

28 J. Tang, R. R. Salunkhe, J. Liu, N. L. Torad, M. Imura, S. Furukawa and Y. Yamauchi, Thermal Conversion of Core-Shell Metal-Organic Frameworks: A New Method for Selectively Functionalized Nanoporous Hybrid Carbon, *J. Am. Chem. Soc.*, 2015, **137**, 1572.

29 J. Yang, F. J. Zhang, H. Y. Lu, X. Hong, H. L. Jiang, Y. E. Wu and Y. D. Li, Hollow Zn/Co ZIF Particles Derived from Core-Shell ZIF-67@ZIF-8 as Selective Catalyst for the Semi-

Hydrogenation of Acetylene, *Angew. Chem., Int. Ed.*, 2015, **54**, 10889.

30 S. Furukawa, K. Hirai, K. Nakagawa, Y. Takashima, R. Matsuda, T. Tsuruoka, M. Kondo, R. Haruki, D. Tanaka, H. Sakamoto, S. Shimomura, O. Sakata and S. Kitagawa, Heterogeneously Hybridized Porous Coordination Polymer Crystals: Fabrication of Heterometallic Core-Shell Single Crystals with an In-Plane Rotational Epitaxial Relationship, *Angew. Chem., Int. Ed.*, 2009, **121**, 1798.

31 X. Yang, S. Yuan, L. F. Zou, H. Drake, Y. M. Zhang, J. S. Qin, A. Alsalme and H. C. Zhou, One-Step Synthesis of Hybrid Core-Shell Metal-Organic Frameworks, *Angew. Chem., Int. Ed.*, 2018, **57**, 3927.

32 S. Choi, T. Kim, H. Ji, H. J. Lee and M. Oh, Isotropic and Anisotropic Growth of Metal-Organic Framework (MOF) on MOF: Logical Inference on MOF Structure Based on Growth Behavior and Morphological Feature, *J. Am. Chem. Soc.*, 2016, **138**, 14434.

33 T. Y. Luo, C. Liu, X. Y. Gan, P. F. Muldoon, N. A. Diemler, J. E. Millstone and N. L. Rosi, Multivariate Stratified Metal-Organic Frameworks: Diversification Using Domain Building Blocks, *J. Am. Chem. Soc.*, 2019, **141**, 2161.

34 D. Mutruc, A. G. Hanssens, S. Fairman, S. Wahl, C. K. Zimathies and S. Hecht, Modulating Guest Uptake in Core-Shell MOFs with Visible Light, *Angew. Chem., Int. Ed.*, 2019, **58**, 12862.

35 T. Li, J. E. Sullivan and N. L. Rosi, Design and Preparation of a Core-Shell Metal-Organic Framework for Selective CO_2 Capture, *J. Am. Chem. Soc.*, 2017, **56**, 15864.

36 K. Ikigaki, K. Okada, Y. Tokudome, T. Toyao, P. Falcaro, C. J. Doonan and M. Takahashi, MOF-on-MOF: Oriented Growth of Multiple Layered Thin Films of Metal-Organic Frameworks, *Angew. Chem., Int. Ed.*, 2019, **58**, 6886.

37 B. Y. Guan, L. Yu and X. W. Lou, A Dual-Metal-Organic-Framework Derived Electrocatalyst for Oxygen Reduction, *Energy Environ. Sci.*, 2016, **9**, 3092.

38 Y. F. Gu, Y. N. Wu, L. C. Li, W. Chen, F. T. Li and S. Kitagawa, Controllable Modular Growth of Hierarchical MOF-on-MOF Architectures, *Angew. Chem., Int. Ed.*, 2017, **129**, 15864.

39 F. I. Pambudi, M. W. Anderson and M. P. Attfield, Unveiling the Mechanism of Lattice-Mismatched Crystal Growth of A Core-Shell Metal-Organic Framework, *Chem. Sci.*, 2019, **10**, 9571.

40 S. Furukawa, K. Hirai, Y. Takashima, K. Nakagawa, M. Kondo, T. Tsuruoka, O. Sakata and S. Kitagawa, A Block PCP Crystal: Anisotropic Hybridization of Porous Coordination Polymers by Face-Selective Epitaxial Growth, *Chem. Commun.*, 2009, **37**, 5097.

41 K. Hirai, K. Chen, T. Fukushima, S. Horike, M. Kondo, N. Louvain, C. Kim, Y. Sakata, M. Meilikhov, O. Sakata, S. Kitagawa and S. Furukawa, Programmed crystallization via epitaxial growth and ligand replacement towards hybridizing porous coordination polymer crystals, *Dalton Trans.*, 2013, **42**, 15868.

42 C. T. Abrahams, B. F. Abrahams, T. A. Hudsonb and R. Robson, Templation of a square grid copper(II) 4,4′-bipyridine network by a 3D PtS-related Cu(I)–Cu(II) 4,4′-bipyridine crystal, *Chem. Commun.*, 2016, **52**, 609.

43 M. D. Hardi, C. Serre, T. Frot, L. Rozes, G. Maurin, C. Sanchez and G. Férey, A New Photoactive Crystalline Highly Porous Titanium (IV) Dicarboxylate, *J. Am. Chem. Soc.*, 2009, **131**, 10857.

44 K. S. Park, Z. Ni, A. P. Côté, J. Y. Choi, R. D. Huang, F. J. U. Romo, H. K. Chae, M. O'Keeffe and O. M. Yaghi, Exceptional Chemical and Thermal Stability of Zeolitic Imidazolate Frameworks, *Proc. Natl. Acad. Sci. U. S. A.*, 2006, **27**, 10186.

45 C. L. Tan, J. Z. Chen, X. J. Wu and H. Zhang, Epitaxial Growth of Hybrid Nanostructures, *Nat. Rev. Mater.*, 2018, **3**, 17089.

46 S. Conrad, P. Kumar, F. Xue, L. M. Ren, S. Henning, C. H. Xiao, K. A. Mkhoyan and M. Tsapatsis, Controlling Dissolution and Transformation of Zeolitic Imidazolate Frameworks by using Electron-Beam-Induced Amorphization, *Angew. Chem., Int. Ed.*, 2018, **57**, 13592.

47 M. T. Zhao, Y. X. Wang, Q. L. Ma, Y. Huang, X. Zhao, J. F. Ping, Z. C. Zhang, Q. P. Lu, Y. F. Yu, H. Xu, Y. L. Zhao and H. Zhang, Ultrathin 2D Metal–Organic Framework Nanosheets, *Adv. Mater.*, 2015, **27**, 7372.

48 J. Cravillon, R. Nayuk, S. Springer, A. Feldhoff, K. Huber and M. Wiebcke, Controlling Zeolitic Imidazolate Framework Nano-and Microcrystal Formation: Insight into Crystal Growth by Time-Resolved in Situ Static Light Scattering, *Chem. Mater.*, 2011, **23**, 2130.

49 C. Avci, J. Ariñez-Soriano, A. Carné-Sánchez, V. Guillerm, C. Carbonell, I. Imaz and D. Maspoch, Post-Synthetic Anisotropic Wet-Chemical Etching of Colloidal Sodalite ZIF Crystals, *Angew. Chem., Int. Ed.*, 2015, **54**, 14417.

50 Y. Chen and J. Washburn, Structural Transition in Large-Lattice-Mismatch Heteroepitaxy, *Phys. Rev. Lett.*, 1996, **77**, 4046.

51 F. Guo, J. H. Guo, P. Wang, Y. S. Kang, Y. Liu, J. Zhao and W. Y. Sun, Facet-dependent photocatalytic hydrogen production of metal–organic framework NH_2-MIL-125(Ti), *Chem. Sci.*, 2019, **10**, 4834.

52 S. Z. Li, W. X. Shi, G. Lu, S. Z. Li, S. C. J. Loo and F. W. Huo, Unconventional Nucleation and Oriented Growth of ZIF-8 Crystals on Non-Polar Surface, *Adv. Mater.*, 2012, **24**, 5954.

53 H. Assi, G. Mouchaham, N. Steunou, T. Devic and C. Serre, Titanium Coordination Compounds: from Discrete Metal Complex-es to Metal-Organic Frameworks, *Chem. Soc. Rev.*, 2017, **46**, 3431.

54 O. Karagiaridi, M. B. Lalonde, W. Bury, A. A. Sarjeant, O. K. Farha and J. T. Hupp, Opening ZIF-8: A Catalytically Active Zeolitic Imidazolate Framework of Sodalite Topology with Unsubstituted Linkers, *J. Am. Chem. Soc.*, 2012, **134**, 18790.

55 M. Sanlés-Sobrido, M. Pérez-Lorenzo, B. Rodríguez-González, V. Salgueiriño and M. A. Correa-Duarte, Highly Active Nanoreactors: Nanomaterial Encapsulation Based on Confined Catalysis, *Angew. Chem., Int. Ed.*, 2012, **51**, 3877.

56 S. H. A. M. Leenders, R. G. Doria, B. D. Bruin and J. N. H. Reek, Transition Metal Catalysis in Confined Spaces, *Chem. Soc. Rev.*, 2015, **44**, 433.

57 C. Perego and R. Millini, Porous Materials in Catalysis: Challenges for Mesoporous Materials, *Chem. Soc. Rev.*, 2013, **42**, 3956.

